Annals of Botany **133**: 321–335, 2024
https://doi.org/10.1093/aob/mcad188, available online at www.academic.oup.com/aob

ANNALS OF BOTANY
Nonprofit since 1887

Mechanisms of grapevine resilience to a vascular disease: investigating stem radial growth, xylem development and physiological acclimation

Ninon Dell'Acqua[1], Gregory A. Gambetta[2], Sylvain Delzon[3], Nathalie Ferrer[1], Laurent J. Lamarque[3,4], Nicolas Saurin[5], Pauline Theodore[1] and Chloé E. L. Delmas[1,*]

[1]INRAE, Bordeaux Sciences Agro, ISVV, SAVE, F-33140, Villenave d'Ornon, France, [2]EGFV, Bordeaux-Sciences Agro, INRAE, Université de Bordeaux, ISVV, 210 chemin de Leysotte, 33882 Villenave d'Ornon, France, [3]Univ. Bordeaux, INRAE, BIOGECO, 33615 Pessac, France, [4]Département des Sciences de l'Environnement, Université du Québec à Trois-Rivières, Trois-Rivières, Canada and [5]UE Pech Rouge, Univ Montpellier, INRAE, Gruissan, France
[*]For correspondence: E-mail chloe.delmas@inrae.fr

Received: 19 October 2023 Returned for revision: 9 November 2023 Editorial decision: 1 December 2023 Accepted: 7 December 2023

• **Background and Aims** Plant vascular diseases significantly impact crop yield worldwide. Esca is a vascular disease of grapevine found globally in vineyards which causes a loss of hydraulic conductance due to the occlusion of xylem vessels by tyloses. However, the integrated response of plant radial growth and physiology in maintaining xylem integrity in grapevine expressing esca symptoms remains poorly understood.
• **Methods** We investigated the interplay between variation in stem diameter, xylem anatomy, plant physiological response and hydraulic traits in two widespread esca-susceptible cultivars, 'Sauvignon blanc' and 'Cabernet Sauvignon'. We used an original experimental design using naturally infected mature vines which were uprooted and transplanted into pots allowing for their study in a mini-lysimeter glasshouse phenotyping platform.
• **Key Results** Esca significantly altered the timing and sequence of stem growth periods in both cultivars, particularly the shrinkage phase following radial expansion. Symptomatic plants had a significantly higher density of occluded vessels and lower leaf and whole-plant gas exchange. Esca-symptomatic vines showed compensation mechanisms, producing numerous small functional xylem vessels later in development suggesting a maintenance of stem vascular cambium activity. Stabilization or late recovery of whole-plant stomatal conductance coincided with new healthy shoots at the top of the plant after esca symptoms plateaued.
• **Conclusions** Modified cropping practices, such as avoiding late-season topping, may enhance resilience in esca-symptomatic plants. These results highlight that integrating dendrometers, xylem anatomy and gas exchange provides insights into vascular pathogenesis and its effects on plant physiology.

Key Words: Dendrometer, esca, gas exchange, grapevine, plant hydraulics, radial growth, vascular disease, xylem anatomy.

INTRODUCTION

Xylem tissue plays a central role in transporting water and nutrients from roots to leaves. This transport occurs in a metastable state under tension (Dixon and Joly, 1894) and is essential for gas exchange, photosynthesis, and thus the growth and productivity of vascular plants. Disrupting the flow of water and nutrients can lead to a decrease in productivity and, if severe, to the death of the plant by hydraulic failure. Negative impacts on the plant hydraulic system can be induced by both abiotic and biotic stresses through a variety of processes (Mensah *et al*., 2020; McDowell *et al*., 2022). However, the impact of biotic stresses on plant hydraulics and the subsequent consequences on plant growth and mortality risk is still an incipient field of study.

Under optimal growth conditions, the long-term radial growth of plants is typically characterized by a rapid growth phase that begins in spring after winter dormancy, followed by a gradual decrease as the growing season progresses (Deslauriers *et al*., 2007; Gruber *et al*., 2018). However, some species such as *Vitis vinifera* deviate from this pattern by undergoing a phase of stem size reduction following the initial rapid growth phase. This shrinkage occurs at the same time as the onset of fruit ripening, and was previously thought to be due to assimilate relocation from the stem to the berries (Intrigliolo and Castel, 2007). However, Van de Wal *et al.* (2018) suggested that stem shrinkage may occur due to the formation of a new periderm layer, followed by dehydration and death of tissues located beyond the newly formed periderm. Although it is widely acknowledged that biotic stresses and dieback processes have an impact on plant growth (e.g. Hartmann and Messier, 2008; Oliva *et al*., 2016; Rizzoli *et al*., 2022), little is known regarding the real-time effects of pest and pathogen infections on stem diameter variations during these specific growth periods (see Cohen *et al*., 1997; Luque *et al*., 1999; Cailleret *et al*., 2017). For example, continuous monitoring of plant growth using stem or trunk radial dendrometers would allow the effects of biotic stresses to be linked to changes in growth, which could be integrated with gas exchange, hydraulics, and anatomy. Multi-trait

approaches are crucial to improve our understanding of short-term changes in plant–pathogen interactions.

Vascular diseases occur worldwide and are caused by destructive plant pathogens (bacterial, fungal or oomycete microorganisms) with dramatic negative impacts on crops (Yadeta and Thomma, 2013). Vascular pathogenesis can cause hydraulic failure through the production of gums or gels (amorphous extracellular materials; Rioux *et al*., 1998), and/or tyloses. Tyloses are vascular parenchyma invaginations within xylem vessels (Pearce, 1996). These vessel occlusions presumably support compartmentalization after injury and limit the spread of wood decay organisms and pathogens, especially vascular pathogens (De Micco *et al*., 2016). However, different vascular host–pathogen interactions have shown that vessel occlusions such as tyloses can alter water transport, decreasing hydraulic conductivity (Collins *et al*., 2009; Urban and Dvořák, 2014; Mensah *et al*., 2020; Bortolami *et al*., 2021*a*). These occlusions may be associated with a decrease in stomatal conductance (Bortolami *et al*., 2021*b*; Fanton *et al*., 2022) or not (Mensah *et al*., 2020) probably depending on the specific plant–pathogen interaction. Recently, X-ray microtomography visualization of xylem vessels in esca-symptomatic grapevines revealed hydraulic failure due to the presence of tylose and/or gel in the lumen of leaf vessels, at distance from the pathogen location in the trunk (Bortolami *et al*., 2019). Different organs appear to be differentially impacted by these vascular occlusions. The highest level of hydraulic failure was found in the peripheral veins of esca-symptomatic leaf blades with a 79 % loss of functional xylem tissue on average, as estimated using the optical vulnerability technique (Bortolami *et al*., 2023). Using *in vivo* X-ray microtomography visualizations, the loss of hydraulic conductance measured in the midrib was 69 % on average, 55 % in the petiole, and 27.5 % in the symptomatic current year shoot (Bortolami *et al*., 2019, 2021*a*). At the same time stomatal conductance and CO_2 assimilation are reduced in symptomatic leaves (Bortolami *et al*., 2021*b*). In addition, some studies have shown that pathogens have the potential to impact the cambial activity and alter xylem development in grapevine (e.g. during eutypiosis: Rudelle *et al*., 2005; and flavescence dorée: Jelmini *et al*., 2021). We can hypothesize that reduced photosynthesis along with impaired water transport due to tylosis formation during esca pathogenesis could alter radial growth and cambial activity in symptomatic stems. A better understanding of the distribution of occluded vessels within the xylem of healthy and symptomatic shoots could help identify their role in pathogenesis and their impact on plant growth and water relationships.

The aim of this study was to examine the impact of the vascular disease esca on stem growth dynamics, xylem anatomy and physiology in two susceptible widespread grapevine cultivars, 'Sauvignon blanc' and 'Cabernet Sauvignon'. More specifically, we developed a multi-trait and integrative approach to monitor vascular pathogenesis and assess the putative resilience capacity of esca-symptomatic plants. Esca is a vascular disease of grapevine with significant negative economic impacts on viticulture (Hofstetter *et al*., 2012; Bruez *et al*., 2013). Although esca has been recognized for more than 100 years (Mugnai *et al*., 1999), it is still poorly understood, mainly because it is not yet possible to reliably reproduce the development of leaf symptoms by pathogen inoculation in the laboratory. To study esca pathogenesis under controlled conditions, we used an original experimental design consisting of naturally infected 20-year-old plants uprooted from two vineyards in France and transplanted into pots. Multiple traits were monitored during 3 months in the glasshouse: plant-water relations at the leaf and whole-plant scales (measuring whole-plant and leaf gas exchange, and predawn and midday water potentials), continuous stem radial growth (using dendrometer measurements), xylem anatomy and tylose formation (through optical microscopy of stem and midrib cross-sections), and esca leaf symptom expression.

MATERIALS AND METHODS

Plant material

Twenty-year-old plants of two *Vitis vinifera* cultivars were uprooted in winter 2021 from two Bordeaux vineyards: nine plants of 'Sauvignon blanc' grafted on Fercal from Couhins (44°45′17.9″N, 0°33′32.6″W) and ten plants of 'Cabernet Sauvignon' grafted on 101-14MGt from Luchey-Halde (44°49′25.4″N, 0°37′51.4″W). Leaf symptoms have been monitored on each plant since 2012. All selected vines had expressed esca leaf symptoms at least once since 2012. We considered plants that did not express symptoms in 2021 as controls, as we previously demonstrated that the history of leaf symptom expression in the past had no significant impact on plant physiological and hydraulic traits (Bortolami *et al*., 2021*b*).

We uprooted the vines in March 2021 and transferred them into 20-L pots following the protocol detailed in Bortolami *et al*. (2019). Outside of the field environment, transplanting vines is the only method allowing for the study of natural esca symptom development on mature plants. Before the beginning of the experimentation, inflorescences were removed to homogenize the plant material, and during the experimentation secondary shoots were removed just after budbreak, except for the most apical secondary shoot after pruning. In the glasshouse, plants were irrigated with nutrient solution [0.1 mM $NH_4H_2PO_4$, 0.187 mM NH_4NO_3, 0.255 mM KNO_3, 0.025 mM $MgSO_4$, 0.002 mM Fe, and oligo-elements (B, Zn, Mn, Cu and Mo)]. Environmental conditions were monitored every 15 min using temperature and humidity probes (S-THB-M002, Onset) and global radiation sensors (S-LIx-M003, Onset) connected to a data logger (U300-NRC, Onset) and installed 1 m above the plants in the glasshouse. The 19 plants were randomly installed in the three rows in a mini-lysimeter glasshouse phenotyping platform (Bord'O platform, INRAE Bordeaux), alternating the cultivar, on individual scales (CH15R11, OHAUS type CHAMP) measuring their weight continuously during 4 months between 9 June and 1 October 2021. To avoid any water stress, plants were automatically watered to field capacity twice a day (at 0800 and 2000 h). The field capacity was determined by immerging the plants into water for 15 min, draining and then weighing on the day before launching the experimentation. To measure only plant transpiration, the pots were sealed with bags during the whole experimental period.

Esca leaf symptom monitoring

Leaf symptom onset and evolution were monitored weekly over a 3-month period at the leaf, current year shoot and whole plant levels (Supplementary Data Fig. S1). At the end of the experimentation five out of nine 'Sauvignon blanc' and seven out of ten 'Cabernet Sauvignon' vines were symptomatic. The leaf symptoms were separated into three classes: 'C', green leaves on control plants (asymptomatic between June and October 2021); 'AS', green leaves from symptomatic plants (both before and after symptom appearance); and 'S', symptomatic leaves (presenting tiger-stripe leaves) on symptomatic plants. Likewise, stems from control plants were named 'C' and stems with symptomatic leaves 'S'.

Stem growth measurements

Stem diameter dynamics was continuously monitored on 11 vines randomly chosen ($n = 6$ 'Sauvignon blanc' and $n = 5$ 'Cabernet Sauvignon') using stem dendrometers (DD-S2 Dendrometer, Ecomatik). Plants were pruned to keep four spurs for each of the two arms, and one bud for each spur was selected. Each dendrometer was installed on a randomly chosen stem among the eight stems, on the first basal internode that was long and strong enough to support it. Trunk radial growth was also measured in four vines using trunk dendrometers installed in the middle part of the trunk. All dendrometers were connected to data-loggers (DL-18, Dendrometer data logger, Ecomatik) and the data were retrieved weekly via HOBOware software. Data were recorded on a 60-min schedule continuously from end of June to end of September. The raw dendrometer data of each vine were checked and cleaned using the 'treenetproc' package via the R software (v.4.2.2) and its three main steps and functions. At the end of this cleaning procedure and as the dendrometers are placed at the beginning of the season without knowing stem symptom evolution, growth analysis had to be performed on one control and four symptomatic 'Cabernet Sauvignon' stems, and three control and three symptomatic 'Sauvignon blanc' stems.

Different growth parameters were calculated for different time intervals: (1) maximum diameter of a day (*MXD*, in µm) which was normalized by the first value measured by the dendrometer to obtain comparable, size-independent measurements of dimensional changes (as done by Scholz *et al*., 2008); (2) daily growth rate (*DGR*, in µm) which is the difference between the maximum diameter between two consecutive days; and (3) weekly average *DGR* (DGR_W, in µm). Based on the patterns of DGR_W over the season and literature (Van de Wal *et al*., 2018), and for further analysis, we separated the growing season into three periods: the stem growth period (before week 29, '*GR*'); the shrinkage period (between weeks 30 and 33, '*SH*') and the stabilization period at the end of the growing season (between weeks 34 and 39, '*ST*').

Xylem anatomy analysis

Stem cross-sections. At the end of the experimentation, one stem per plant that was not equipped with any dendrometers was selected (symptomatic stems from esca-symptomatic plants and asymptomatic stems from control plants). Xylem anatomy analysis was then performed on three control and five symptomatic 'Sauvignon blanc' stems and three control and six symptomatic 'Cabernet Sauvignon' stems. All stems had a maximum percentage of symptomatic leaves above 55 %, except one 'Sauvignon blanc' stem with 27.8 %. Among these stems, 42 % produced green regrowth after symptom expression. Samples 1 cm long from the 12th node from the base node were stored in 70 % ethanol. Cross-sections 50 µm thick were made using a GSL-1 microtome (Gärtner *et al*., 2014). The sections were placed for about 2 min in a 0.5 % safranin/astrablue solution, rinsed twice with absolute ethanol, impregnated with xylene, and then mounted between slide and coverslip with Histolaque (Histolaque LMR) to obtain permanent slides (three cross-sections per sample). Images of the sections were taken using a binocular magnifier associated with a Nikon SMZ1270 camera, and the NIS-ElementsD software associated with the magnifier. For each sample, we selected the clearest, best coloured and most complete cross-section for analysis.

Stem xylem analysis. The different anatomical traits measured and derived from these measurements for each sample are listed in Table 1 according to Scholz *et al*. (2013). To obtain a more accurate representation of the distribution of the fully or partially

TABLE 1. *Directly measured or derived quantitative xylem anatomical traits*

Acronym	Trait	Unit	Formula	Measurement level
PA	Pith area	µm²	–	Entire cross-section
A_X	Xylem area	µm²	–	Entire cross-section and dorso-ventral area
Av	Xylem vessel area	µm²	–	Entire cross-section and dorso-ventral area
D	Xylem vessel diameter	µm	$2\sqrt{A/\pi}$	Entire cross-section and dorso-ventral area
V_D	Xylem vessel density	no. mm^{-2}	$\frac{no.\ \ vessels}{A_X}$	Entire cross-section and dorso-ventral area (calculated either for occluded or non-occluded vessels)
D_H	Hydraulic diameter	µm	$\frac{\sum D^5}{\sum D^4}$	Entire cross-section
k_{th}	Theoretical hydraulic conductivity	kg s^{-1} m MPa^{-1}	$\frac{\pi D^4 \rho}{128\eta}$	Entire cross-section and dorso-ventral area (calculated either for all, occluded or non-occluded vessels)
k_{ts}	Theoretical specific hydraulic conductivity	kg s^{-1} m^{-1} MPa^{-1}	$\frac{\sum k_{th}}{A_X}$	Entire cross-section and dorso-ventral area (calculated either for all, occluded or non-occluded vessels)
PLC_{th}	Theoretical percentage loss of conductivity	%	$100 \times \frac{\sum k_{th\ occ.\ vessels}}{\sum k_{th\ all\ vessels}}$	Entire cross-section and dorso-ventral area

occluded vessels in the xylem according to cultivar ('Sauvignon blanc', 'Cabernet Sauvignon') and symptoms (esca, control), an additional analysis was performed based on the relative position of each xylem vessel in the dorso-ventral region of each stem (Fig. 1). This process consisted of measuring the distance from the pith for each dorsal and ventral vessel and analysing conduit characters continuously or in bins (of each 20 % distance interval from the pith in the xylem tissue) (Table 1). The area for each stem portion was also measured to calculate vessel density.

Midrib cross-sections. Three 'C', four 'S' and four 'AS' leaves were sampled in 'Sauvignon blanc' and three 'C', five 'AS' and six 'S' leaves in 'Cabernet Sauvignon'. A 1-cm length of the midrib of each leaf was stored in 70 % ethanol. Samples were then fixed in a formalin-aceto-alcohol (FAA) solution for at least 15 h and processed as described in detail in Bortolami *et al*. (2023) with a dehydration phase followed by embedding using a graded series of LR White resin. Cross-sections were of 2 µm were realized in each embedded sample using an ultracut S microtome (Reichert) equipped with a glass knife at the Bordeaux Imaging Center, a member of the France Bio Imaging national infrastructure (ANR-10-INBS-04). The sections were fixed to the slide by placing them on a warm plate and stained with 0.05 % Toluidine blue O to detect the presence of tyloses and gels in the vessel lumens. Images of each section were taken using a binocular magnifier associated with a Nikon SMZ1270 camera, and the NIS-ElementsD software. For each slide, we selected the clearest, best coloured and most complete cross-section for analysis.

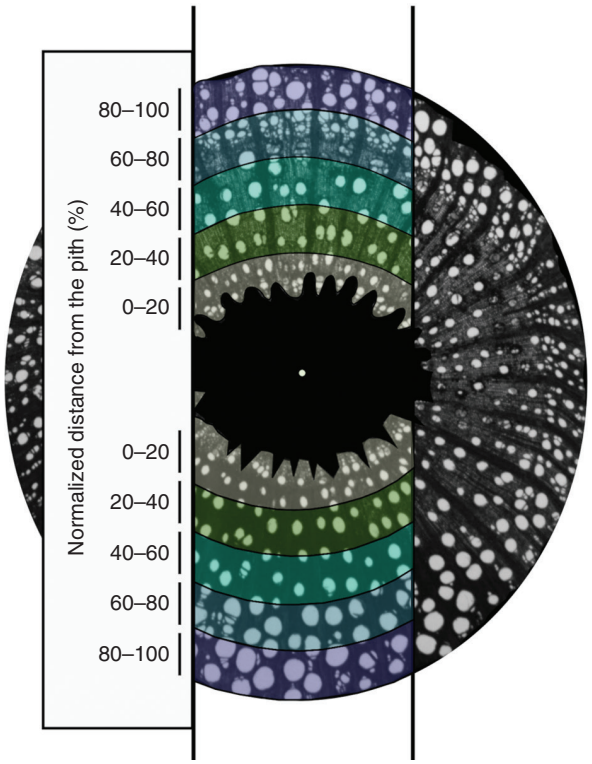

FIG. 1. Simplified representation of the normalized distance from the pith (%). The xylem tissue was separated into five portions according to their normalized distance from the pith (0–20, 20–40, 40–60, 60–80 and 80–100 %). The distance of each vessel was measured from the centre of the pith and then normalized by measuring the vessel closest to and farthest from the pith in the dorsal and ventral regions. The vessels were then grouped according to the xylem portion. The xylem portions are reported in different colours, while the white point represents the pith centre.

Midrib xylem analysis. Using ImageJ software (Image J 1.53t, Wayne Rasband and contributors, National Institutes of Health), the number of occluded and non-occluded vessels were counted to obtain a percentage of vessel occlusion per midrib.

Balance data analysis

Whole-plant transpiration per leaf area (E in mmol m^{-2} s^{-1}) was calculated as follows:

$$E = \frac{\Delta_w}{A_L} \times \frac{1}{MWw}, \quad (1)$$

where Δ_w corresponds to the change in weight within the considered period (g s^{-1}), A_L to the total leaf area of the plant (m^2) and MW_w to the molecular weight of water (18 g mol^{-1}). To avoid aberrant values, Δ_w measurements were considered only when ranging from 0 to –0.5 g s^{-1} which correspond to E values that lie within a reasonable range.

Total leaf area (A_L) was estimated through the relationship obtained between leaf midrib length and leaf area (measured with a Model LI-3000leaf area meter, Li-Cor) for both cultivars using ~150 non-symptomatic leaves per cultivar. The leaf midribs were measured every other week on all the leaves of each plant. In the case of symptomatic plants, the presence of green regrowth was noted and included in the total leaf area. Whole-plant (canopy) conductance (G_C in mmol m^{-2} s^{-1}), was then calculated as:

$$G_C = K_G(T) \times \frac{E}{D}, \quad (2)$$

where $K_G(T)$ corresponds to the conductance coefficient ($115.8 + 0.4236T$, kPa m^3 kg^{-1}), E to the transpiration (mmol m^{-2} s^{-1}), and D to the vapour pressure deficit (kPa) calculated using relative humidity (%) and T (°C) from climatic records. The G_C values were only used when radiation was saturating for photosynthesis [photosynthetic photon flux density (PPDF) > 700 µmol m^{-2} s^{-1}] and when $D \geq 0.6$ kPa (Ewers and Oren 2000). In addition, errors in G_C estimates were kept to less than 10 %.

Water potential

The minimum leaf water potential (between 1300 and 1500 h) was measured weekly on mature well-exposed leaves from the middle of the stem, between June and September (12 measuring dates) with a pressure chamber (Scholander). For symptomatic plants, the water potential was measured only in AS leaves, to avoid an artefact measurement due to the occlusions of vessels by tyloses.

Gas exchange

Gas exchange measurements were made between 0900 and 1200 h on mature well-exposed leaves using the TARGAS-1 portable photosynthesis system (PP Systems). Optimal

conditions of photosynthetically active radiation were set in the cuvette (1500 µmol m^{-2} s^{-1}). Maximal CO_2 assimilation, A_{max} (µmol m^{-2} s^{-1}) was recorded on one (or two for symptomatic plants: 'AS' and 'S') mature well-exposed leaf from the middle of the stem and by alternating the grape cultivars. The measurements were performed weekly on each of the 19 plants, for ten measuring dates, between 16 June and 17 August 2021, gathering together 62 'C' leaves, 42 'S' leaves and 29 'AS' leaves.

Ambient stomatal conductance was measured weekly between 21 July and the 22 September 2021, with the Li-600 (Li-Cor) on the green surface of asymptomatic and symptomatic mature well-exposed leaves. The measurements were made between 1000 and 1200 h on each of the 19 plants, for ten measuring dates, gathering together 69 control leaves from control asymptomatic plants, 79 symptomatic and 36 green asymptomatic leaves from symptomatic plants.

Statistical analysis

DGR_W was analysed using a linear mixed-effects model with plant parameter set as a random effect and period (GR, SH, ST), esca symptoms (control, esca) and their interactions as fixed effects. A post-hoc Tukey test adjustment for multiple comparisons was also used. We only performed statistical analysis for 'Sauvignon blanc' DGR_W values as only one control stem could be monitored in 'Cabernet Sauvignon'.

Anatomical characteristics of stem xylem and the percentage of occluded vessels in stems and midribs were compared between control plants of the two cultivars, and between control and symptomatic plants within each cultivar, using ANOVAs. We performed Levine's test to verify the equality of the variance. Vessel diameter curves were obtained by using the loess smoothing method.

Vessel density ($V_{D\ occ.\ vessels}$ and $V_{D\ non\ occ.\ vessels}$), vessel size distribution, theoretical specific hydraulic conductivity ($k_{ts\ all\ vessels}$, $k_{ts\ non\ occ.\ vessels}$ and $k_{ts\ occ.\ vessels}$) and PLC_{th} (theoretical percentage loss of conductivity) were analysed using linear mixed-effects models with plant entered as a random effect, and the percentage distance interval from the pith ([0,20], (20,40], (40,60], (60,80] and (80,100]), esca symptoms (control, esca), cultivar ('Sauvignon blanc', 'Cabernet Sauvignon') and their interactions as fixed effects. The data were log transformed after examining residual plots. For data with significant zeros we used the function log1p (package SparkR) to carry out the transformation. Leaf gas exchange (g_s and A) and midday water potentials were analysed with linear mixed-effects models with plant entered as a random effect, since several measurements were performed on the same plant over the season, and cultivar, esca symptoms and their interactions entered as fixed effects. A post-hoc Tukey test adjustment for multiple comparisons was made. Whole-plant stomatal conductance (G_C) curves were obtained by using the loess smoothing method. All statistical analyses were performed using R (v.4.2.2) and are presented in Supplementary Data Tables S1–S8.

RESULTS

Esca leaf symptom incidence

During the course of the experiment, five 'Sauvignon blanc' and seven 'Cabernet Sauvignon' plants exhibited esca leaf symptoms, with first symptom expression occurring between 5 July and 2 August 2021. The maximum percentage of symptomatic leaves for these plants ranged from 27.7 to 100 % per plant, with at least one stem per plant showing more than 75 % leaf symptoms. The remaining four 'Sauvignon blanc' and three 'Cabernet Sauvignon' plants remained asymptomatic and showed no esca leaf symptoms.

Growth and stem diameter variation

Regardless of the cultivar, stem diameter variation from control plants (C1, C2, C3 and C4 stems; Fig. 2, left panel) followed the same growth evolution. The first period is characterized by a fast increase in *MXD* with time, occurring at the beginning of the growing season, until the stems reached a maximum diameter (ΔD_{max}) at the end of July (Fig. 2). The control 'Cabernet Sauvignon' stem reached ΔD_{max} on 1 August 2021 (1088.72 µm, C1; Fig. 2, left panel). 'Sauvignon blanc' ΔD_{max} values ($n = 3$ stems, C2, C3 and C4; Fig. 2, left panel) were lower than the 'Cabernet Sauvignon' stem and staggered between 22 July (580.64 µm, C3, Fig. 2, left panel) and 28 July (713 µm, C2, the maximum value in 'Sauvignon blanc' control plants, Fig. 2, left panel). The second period is characterized by a decrease in *MXD* with time until ΔD_{max} stabilized during the third period of the growing season.

In contrast, after the growth period, the timing, length and intensity of the shrinkage period was highly irregular from one symptomatic stem to another, deviating from the consistent pattern observed in control stems (Fig. 2). In two plants (S6 and S7; Fig. 2, right panel), several periods of shrinkage were observed. In others (e.g. S2, S3 and S5; Fig. 2, right panel), ΔD_{max} was observed later or the maximum stage was prolonged, S1 had no shrinkage period, and finally S4 presented the same pattern as the controls (Fig. 2, left and right panels).

The small number of reliable trunk dendrometers does not allow conclusions about the growth response of the trunk ($n = 1$ control and $n = 3$ symptomatic plants; Supplementary Data Fig. S2). However, we observed similar patterns between trunk and stem growth responses. For example, plant S1 increased growth at the end of the season in both stem and trunk organs. A stall in the growth of both the stem and trunk of plant S5 was also observed, thus reinforcing the fact that this observation did not result from a measurement artefact. Finally, the only exploitable control trunk dendrometer (C2; Fig. S2, left panel) showed the same growth pattern as the control stems characterized by the three phases of growth, shrinkage and finally stabilization. Comparing the trunk and stem curves of the control plant (C2), we found a larger and longer growth phase in the trunk as well as a later transition to the shrinkage phase (mid-August in the stem, end of August in the trunk).

Growth rate dynamics over the season

The three growth periods were precisely defined using the evolution of DGR_W over time in control stems (Fig. 3): positive DGR_W values were associated with the GR period (before week 29), negative values with the SH period (between weeks 30 and 33), and values close to zero at the stabilization period at end of the season ('ST', between weeks 34 and 39).

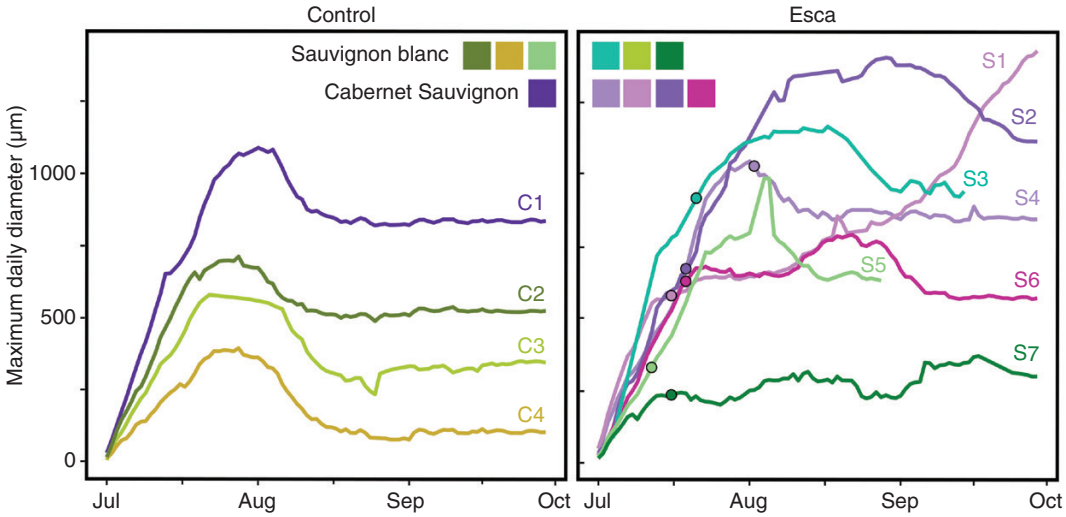

FIG. 2. Evolution of the stem standardized maximum daily diameter (*MXD*, µm) in symptomatic and control stems over one vegetative season in *Vitis vinifera* cv. 'Sauvignon blanc' and 'Cabernet Sauvignon'. Control 'Sauvignon blanc' (C2, C3, C4) and 'Cabernet Sauvignon' (C1) stems are shown in the left panel and symptomatic 'Sauvignon blanc' (S3, S5, S7) and 'Cabernet Sauvignon' (S1, S2, S4, S6) stems in the right panel. Points on the curves correspond to the dates of symptom onset.

Overall, DGR_W over the season was visually similar between cultivars, despite higher values during the GR period in 'Cabernet Sauvignon' (Fig. 3). In 'Sauvignon blanc', period and the interaction between period and esca symptoms had a significant impact on DGR_W (Supplementary Data Table S1). The DGR_W of control and symptomatic plants did not differ significantly during the GR and ST periods (Fig. 3; $P > 0.05$, Tukey test). However, during the SH period, the DGR_W of control stems was significantly lower (i.e. higher shrinkage) than that of symptomatic stems (Fig. 3(i); $P = 0.01$). The same trend was observed in 'Cabernet Sauvignon' although only one control stem could be monitored.

Xylem anatomical analysis

Stem xylem anatomy. Among control plants, pith area (*PA*), xylem area (A_x) and vessel density (V_D) did not differ significantly between cultivars (Supplementary Data Table S2). Hydraulic diameter was significantly higher in 'Sauvignon blanc' ($D_H = 153.5 \pm 13.3$ µm) than in 'Cabernet Sauvignon' ($D_H = 84.5 \pm 12.2$ µm), resulting in a four times higher theoretical hydraulic conductivity (k_{ts}) in 'Sauvignon blanc' control stems (Fig. S3, Table S2).

Symptomatic and control stems did not present significant differences in *PA*, A_X, V_D, D_H or k_{ts} in 'Cabernet Sauvignon' and 'Sauvignon blanc' for whole stem section analyses (Supplementary Data Table S2).

Vessel occlusion in stems and midribs. The percentage of vessels occluded by tyloses or gels was quantified on stem and midrib cross-sections and was lower than 4 % in control stems and midribs of the two cultivars (Fig. 4). In symptomatic stems, 9.6 ± 1.8 % of xylem vessels were occluded in 'Cabernet Sauvignon' and 25.6 % ± 10.8 % in 'Sauvignon blanc' (Fig. 4A). However, the differences in vessel occlusion between control and symptomatic stems within each cultivar was not significant (Fig. 4A). Note that when selecting only stems with more than 55 % of symptomatic leaves (i.e. removing one stem with 27 % of symptomatic leaves), the percentage of occluded vessels was significantly higher than that of the control stems in 'Sauvignon blanc' ($P = 0.03$, Kruskal–Wallis). At the leaf level, midribs of symptomatic leaves had significantly more occluded vessels than asymptomatic and control leaves in both cultivars (Fig. 4B).

Anatomical trait variability across the xylem area

Vessel density (VD). Vessel density of occluded vessels, $V_{D\ occluded\ vessels}$, differed significantly between intervals across the xylem area and was greatest closest to the pith (0–20 % distance from the pith) in both symptomatic and control plants (Fig. 5; Supplementary Data Table S3). Moreover, $V_{D\ occluded\ vessels}$ differed significantly between symptomatic and control plants (Table S3). Indeed, $V_{D\ occluded\ vessels}$ in symptomatic stems was higher than that of controls in all intervals in 'Sauvignon blanc', and especially in the first two intervals in 'Cabernet Sauvignon' (Fig. 5A).

Vessel density of non-occluded vessels, $V_{D\ non\ occ.\ vessels}$, differed significantly between intervals across the xylem area in control as well as in symptomatic stems (Supplementary Data Table S3). $V_{D\ non\ occ.\ vessels}$ was highest closest to the pith and in the outermost xylem interval in both control and symptomatic plants, regardless of the cultivar (Fig. 5B). Furthermore, we found a significant effect of the interaction between plant symptoms and intervals across the xylem area on $V_{D\ non\ occ.\ vessels}$. In the outermost xylem interval, $V_{D\ non\ occ.\ vessels}$ in esca symptomatic stems was 105 % higher than in control stems in 'Sauvignon blanc' (despite marginally significant differences, $P = 0.05$, Kruskal–Wallis) and 184 % higher in 'Cabernet Sauvignon' ($P = 0.07$, Kruskal–Wallis) (Fig. 5B).

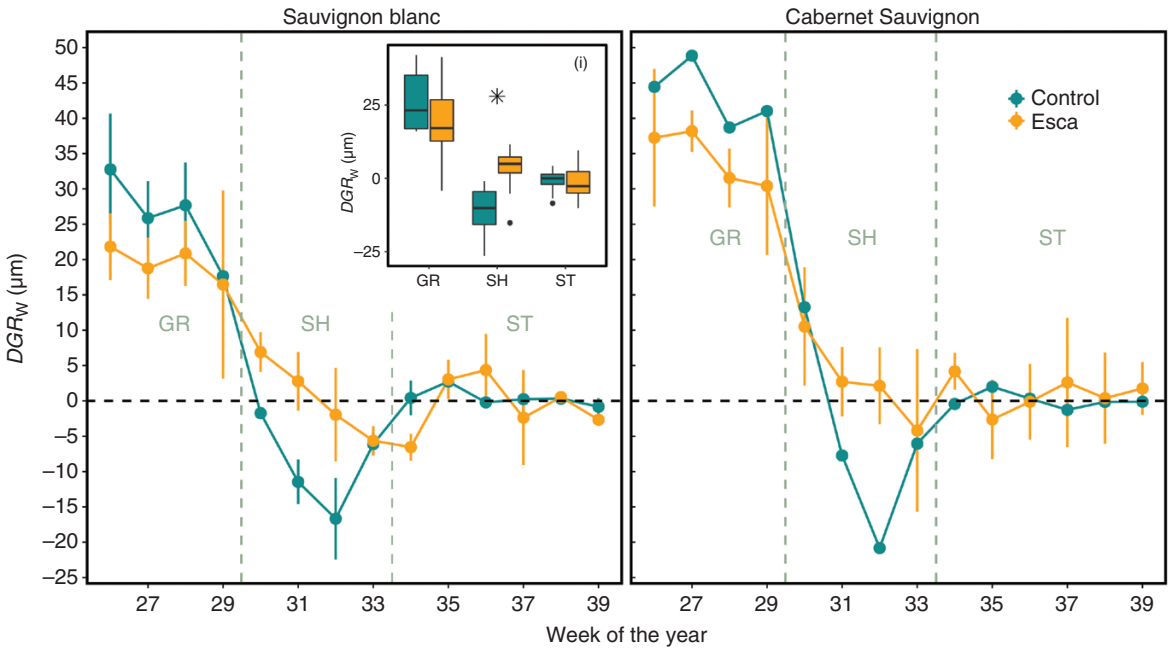

FIG. 3. Mean growth rate (DGR_W, µm) in symptomatic and control stems over weeks in *Vitis vinifera* cv. 'Sauvignon blanc' and 'Cabernet Sauvignon'. Mean growth rate comparison between control stems (green line and dots) and symptomatic stems (yellow line and dots) in 'Sauvignon blanc' (left panel) and 'Cabernet Sauvignon' (right panel). (i) Comparison of the mean growth rate (µm) between control and symptomatic stems of 'Sauvignon blanc' for the three typical growth periods of the control plants: stem growth (before week 29, '*GR*'), shrinkage (between weeks 30 and 33, '*SH*') and stabilization at the end of the season (between weeks 34 and 39, '*ST*'). The vertical bars associated with the data points represent the standard error. The star indicates a significant DGR_W difference between control and symptomatic 'Sauvignon blanc' stems during the SH period ($P = 0.01$, Tukey test).

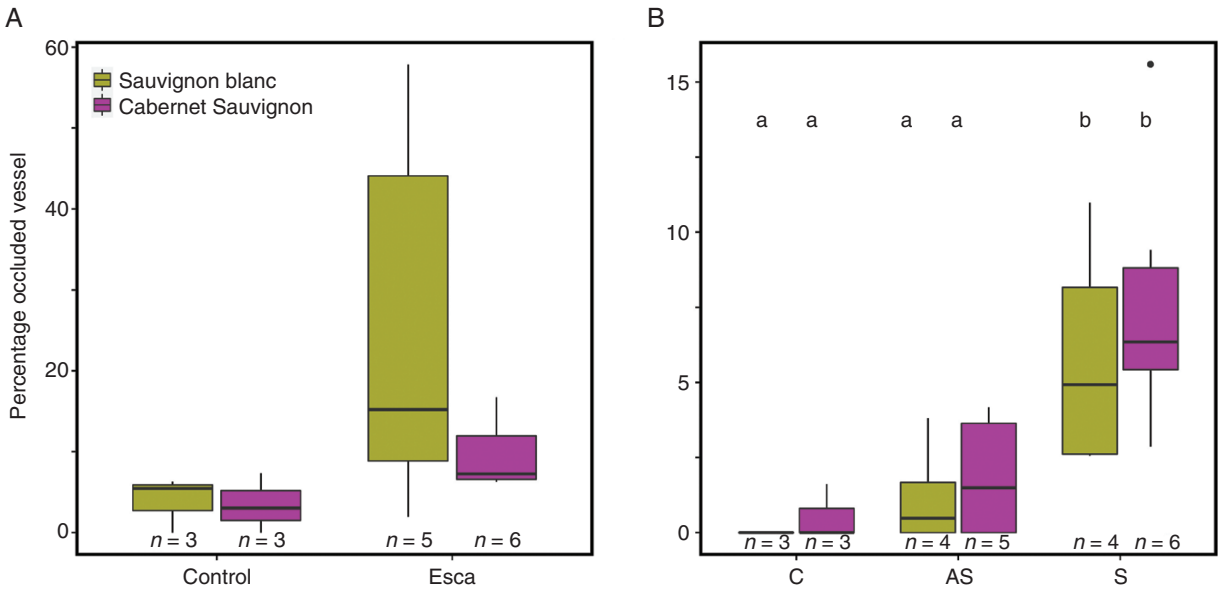

FIG. 4. Percentage of occluded vessels in stems and leaf midribs in *Vitis vinifera* cv. 'Sauvignon blanc' and 'Cabernet Sauvignon' during esca pathogenesis. (A) Percentage of occluded vessels in cross-sections of control and symptomatic stems. No significant differences were found between control and symptomatic stems or between the varieties ($P > 0.05$, ANOVA). (B) Percentage of occluded vessels in midrib cross-sections of control (C), asymptomatic (AS, leaves sampled from a symptomatic plant) and symptomatic (S) leaf midribs. Lower-case letters represent the differences between leaf symptoms within each cultivar and show that green (C and AS) and symptomatic leaves had a significantly different percentage of occlusions in both varieties ($P < 0.05$, ANOVA).

Distribution of vessel size. The distribution of vessel diameter across the xylem area varied significantly according to cultivar, esca symptom expression and distance to pith (Supplementary Data Table S4). Overall, xylem vessel diameters of 'Cabernet Sauvignon' stems were significantly smaller than those of 'Sauvignon blanc' stems (Fig. 6). In particular, in control stems

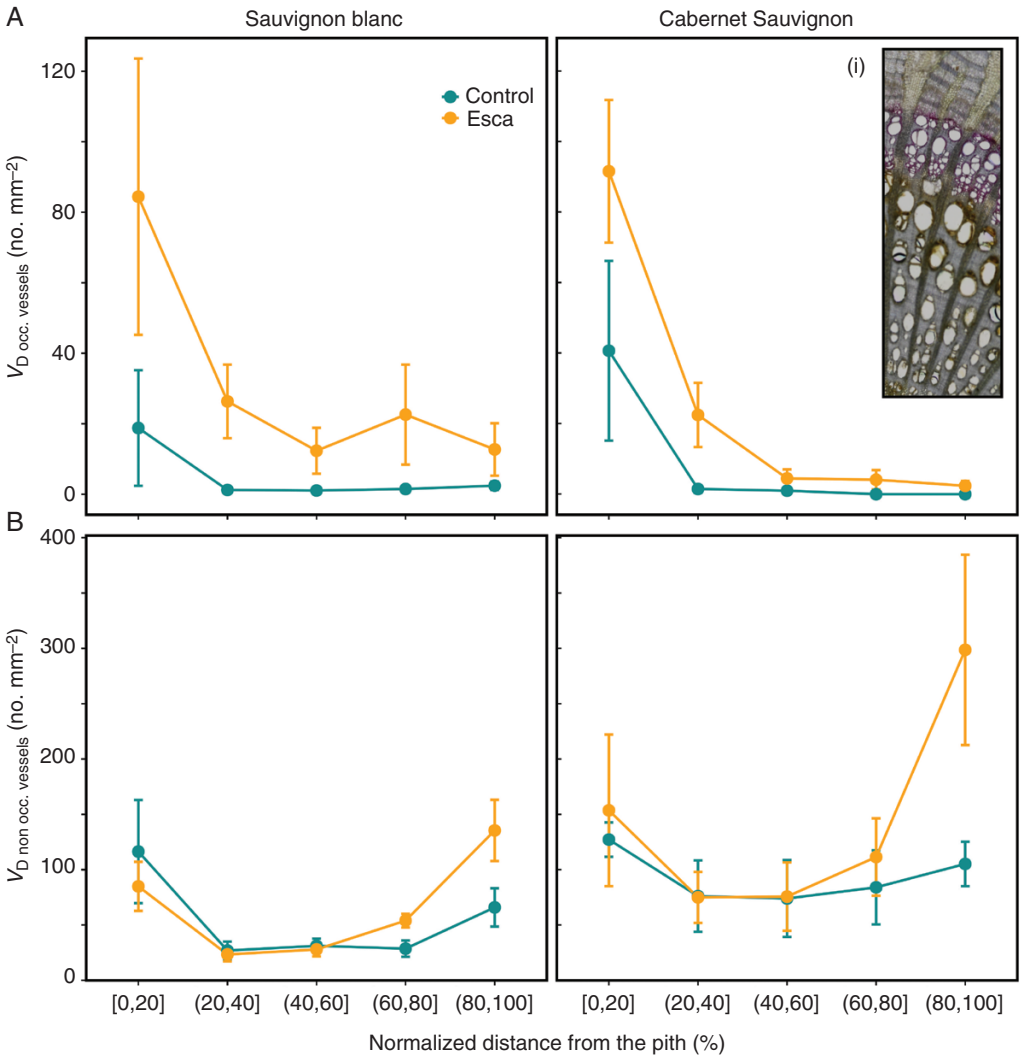

FIG. 5. Distribution of vessel density (V_D) in symptomatic and control stems across the normalized distance from the pith (%) in *Vitis vinifera* cv. 'Sauvignon blanc' and 'Cabernet Sauvignon'. (A) Occluded vessel density (no. mm^{-2}). (B) Non-occluded vessel density (no. mm^{-2}). The distance between the pith and the end of the vascular cambium was separated into 20 % portions and the xylem vessels distributed between them (as presented in Fig. 1), comparing symptomatic stems and control stems in 'Sauvignon blanc' (n = 3 control and n = 5 symptomatic stems, left panel) and in 'Cabernet Sauvignon' (n = 3 control, n = 6 symptomatic stems, right panel). (i) Image of a portion of a dorso-ventral xylem section, stained with phloxine infiltration; pink xylem vessels represent functional vessels. Statistical analyses are presented in Supplementary Data Table S3.

the mean vessel diameter was 44.6 ± 0.9 µm in 'Cabernet Sauvignon' versus 58.4 ± 1.4 µm in 'Sauvignon blanc' and in symptomatic stems 36.8 ± 0.5 µm in 'Cabernet Sauvignon' versus 48.2 ± 0.8 µm in 'Sauvignon blanc'. The vessels with the smallest diameters were located near the pith and in the outermost interval in control plants (Fig. 6). In 'Sauvignon blanc', vessels from symptomatic plants were significantly smaller than those of control 'Sauvignon blanc' plants, especially in the last 50 % distance from the pith. In 'Cabernet Sauvignon', vessels were in the same range of size in symptomatic and control stems until the last 30 % distance from the pith, where the vessels were smaller in symptomatic stems (Fig. 6).

Theoretical specific hydraulic conductivity. The value of $k_{ts\ all\ vessels}$ (including occluded and non-occluded vessels) and $k_{ts\ non\ occ.\ vessels}$ differed significantly between intervals across the xylem area, depending on the cultivar (significant interactions between xylem interval and cultivar, as presented in Supplementary Data Table S5). In 'Sauvignon blanc', the $k_{ts\ all\ vessels}$ and $k_{ts\ non\ occ.\ vessels}$ visually increased towards the interval 60–80 % distance from the pith, before decreasing in the most exterior portion of the xylem tissue, particularly in control stems (Fig. 7A; Fig. S4A). In 'Cabernet Sauvignon', $k_{ts\ all\ vessels}$ was visually consistent across xylem intervals and was significantly lower than in 'Sauvignon blanc' (Fig. 7A; Table S5). The $k_{ts\ all\ vessels}$ and $k_{ts\ non\ occ.\ vessels}$ did not display significant differences between control and symptomatic plants (Table S5). Yet, in symptomatic stems of 'Sauvignon blanc', k_{ts} tended to be lower (the maximum values of $k_{ts\ all\ vessels}$ were 33 % lower in esca-symptomatic plants than those of control plants; Fig. 7A; Fig. S4A).

The $k_{ts\ occ.\ vessels}$ (i.e. corresponding to the theoretical loss of conductivity as also analysed with PLC_{th} below) was

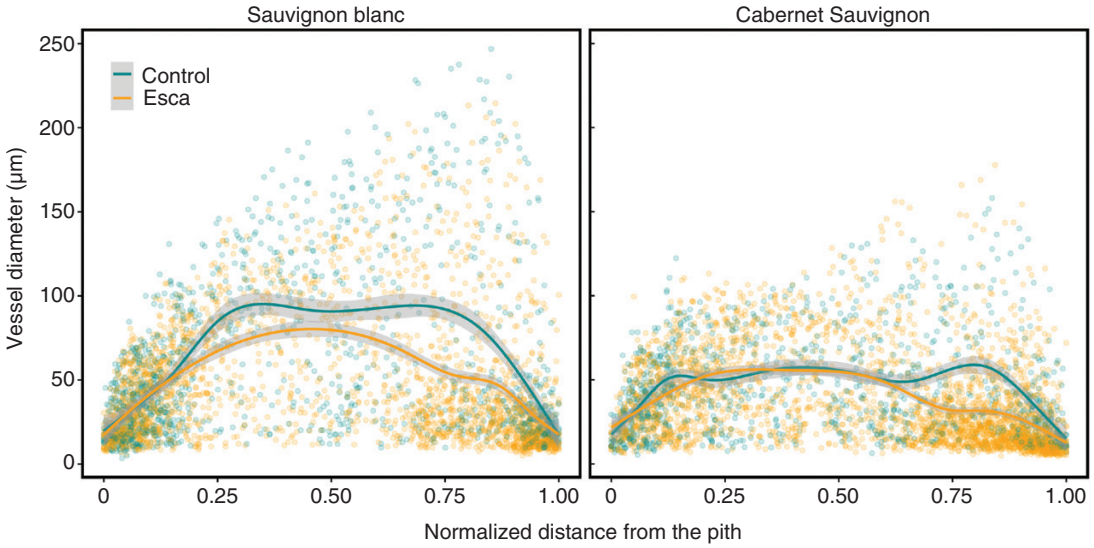

FIG. 6. Repartition of vessel diameter in symptomatic and control stems across the normalized distance from the pith in *Vitis vinifera* cv. 'Sauvignon blanc' and 'Cabernet Sauvignon'. 'Sauvignon blanc' ($n = 3$ control and $n = 5$ symptomatic stems) and 'Cabernet Sauvignon' ($n = 3$ control, $n = 6$ symptomatic stems) are shown in the left and right panels, respectively. Statistical analyses are presented in Supplementary Data Table S4.

significantly different between intervals and between control and symptomatic plants with higher values in symptomatic 'Sauvignon blanc' in all intervals and in the first two intervals in 'Cabernet Sauvignon' (Supplementary Data Fig. S4B, Table S5).

Theoretical percentage loss of conductivity (PLCth). The distribution of PLC_{th} across the xylem tissue intervals differed significantly between control and symptomatic stems (Fig. 7B; Supplementary Data Table S6). In 'Sauvignon blanc', PLC_{th} was greater in symptomatic plants than controls in all intervals and was distributed in a parabolic manner (maximum was 9.2 % ± 4.9 at the interval (40,60] and the minimum was 4.3 % ± 3.2 at the outermost intervals). 'Cabernet Sauvignon' symptomatic stems were characterized by a more localized loss of conductivity within the xylem at the [0,60] interval. Very low levels of PLC_{th} were observed in the outermost intervals of symptomatic 'Cabernet Sauvignon' stems. The highest PLC_{th} in 'Cabernet Sauvignon' controls was localized at the [0,20] interval (3.6 ± 2.3 %).

In whole cross-sections, the theoretical percentages loss of conductivity ($PLC_{th\ all\ section}$) was lower in symptomatic stems compared to control leaves in both varieties but not significantly [Fig. 7B(i and ii)]. Indeed, in 'Sauvignon blanc', $PLC_{th\ all\ section}$ was 0.8 ± 0.5 % in control and 31.9 ± 15 % in symptomatic stems [Fig. 7B(i)]. In 'Cabernet Sauvignon' $PLC_{th\ all\ section}$ was 3.4 ± 2.4 % in control and 16.9 ± 6.8 % in symptomatic stems [Fig. 7B(ii)].

Water relations at leaf and whole plant scale. In both cultivars, whole plant stomatal conductance (G_C) of control plants was relatively stable until the beginning of August and then decreased at the end of the season (Supplementary Data Fig. S5). Overall, G_C of 'Cabernet Sauvignon' control plants was lower than that of 'Sauvignon blanc' on average (Fig. S5).

In symptomatic plants, a decrease in G_C was observed in both cultivars several days prior to the appearance of esca leaf symptoms (necrosis of secondary veins and discoloration of the leaf blade, potentially linked to tissue death). The average daily minimum G_C was reached 8 d after the first symptom observation in 'Cabernet Sauvignon' and 15 d after in 'Sauvignon blanc'. An increase in *Gc* was then observed 3 weeks after the first symptom observation in 'Sauvignon blanc' (Fig. 8A). The G_C of 'Cabernet Sauvignon' stabilized after 1 week until the end of the season (Fig. 8A).

No significant differences between cultivars were found in CO_2 assimilation (A_{max}) and stomatal conductance (g_s) (Supplementary Data Table S7; Fig. 8B and C). Green leaves from symptomatic and control plants (AS and C leaves, respectively) presented similar levels of gas exchange (Table S7; Fig. 8B and C). Symptomatic leaves presented a significantly lower stomatal conductance (g_s) and maximal CO_2 assimilation (A_{max}) than apparently healthy leaves (C and AS) (Table S7; Fig. 8B and C). Midday leaf water potentials were measured along the season on green leaves (water potentials cannot be measured on symptomatic leaves because their xylem vessels are occluded) and did not differ significantly between leaf symptoms and cultivar (Table S8, Fig. S6).

DISCUSSION

In this study we investigated the relationships between stem growth dynamics, physiology and xylem anatomy during esca pathogenesis in two susceptible grapevine cultivars, 'Sauvignon blanc' and 'Cabernet Sauvignon'. In both cultivars, we demonstrated that esca pathogenesis resulted in an alteration in stem growth patterns associated with xylem occlusions in leaves and stems, theoretical loss of conductivity, and a change in stem cambial activity with the production of small functional vessels at the end of the season. Finally, we highlighted that the pathogenesis of esca and varietal differences in xylem anatomy affect gas exchange at both the leaf and whole-plant levels. We found a recovery in whole-plant stomatal conductance 2 weeks after

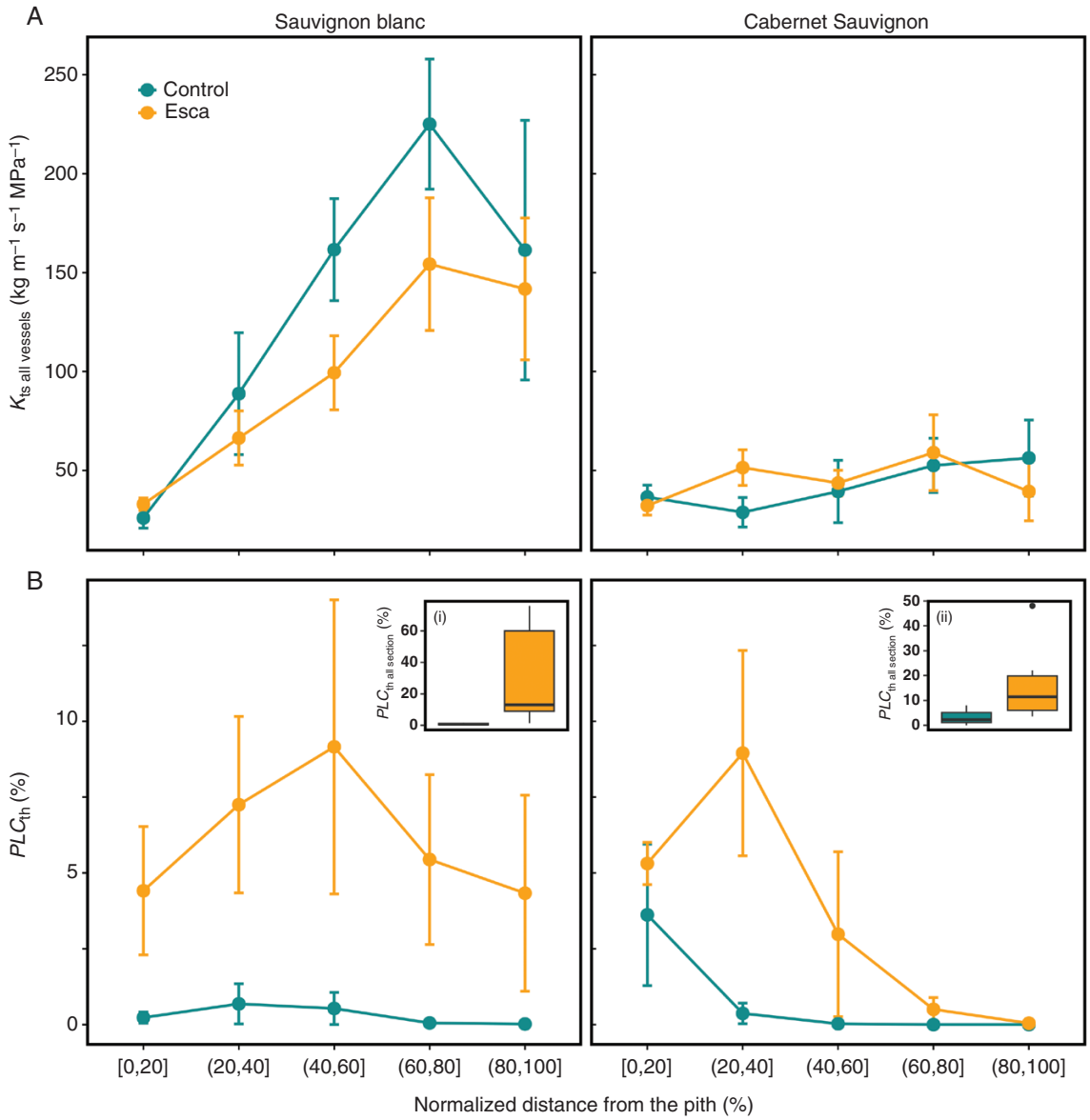

FIG. 7. Theoretical specific hydraulic conductivity and percentage loss of conductivity analysis across the normalized distance from the pith (%) in control and symptomatic stems of *Vitis vinifera* cv. 'Sauvignon blanc' and 'Cabernet Sauvignon'. (A) Theoretical specific hydraulic conductivity estimated using all vessels ($k_{ts\ all\ vessels}$). (B) Percentage loss of conductivity (%; PLC_{th}). The distance between the pith and the end of the vascular cambium was separated into 20 % portions and the xylem vessels distributed between them (as presented in Fig. 1). Each panel shows the comparison between symptomatic and control stems in 'Sauvignon blanc' ($n = 3$ control and $n = 5$ symptomatic stems, left panel) and in 'Cabernet Sauvignon' ($n = 3$ control, $n = 6$ symptomatic stems, right panel). Statistical analyses are presented in Supplementary Data Tables S5 and S6. (i) and (ii) PLC_{th} of 'Sauvignon blanc' and 'Cabernet Sauvignon' whole stem cross-sections, respectively ($P > 0.05$ for both cultivars).

symptom onset in 'Sauvignon blanc' and a stabilization after 1 week in 'Cabernet Sauvignon'. These results shed light on the resilience mechanisms of symptomatic vines, which drive the production of new green leaves and shoots after symptom onset.

Esca leaf symptoms alter stem growth dynamics

Plant growth responses to abiotic stresses, particularly the response of radial growth of stems and trunks to drought stress, have been well studied (Daudet *et al.*, 2005; Fernández and Cuevas 2010). By contrast, studies focused on the influence of vascular disease on seasonal growing patterns are rare (but see Cohen *et al.*, 1997). Radial dendrometers which continuously measure stem or trunk diameters are ideal for monitoring plant growth in real time (Deslauriers *et al.*, 2007). Here we observed the typical pattern of maximum daily diameter (*MXD*) evolution over the season in control plants (successively a growth, a shrinkage and a stabilization period; Fig. 2) (Intrigliolo and Castel, 2007; Conesa *et al.*, 2018; Van de Wal *et al.*, 2018). Additionally it is important to note that the growth pattern of control plants does not appear to be affected by the absence

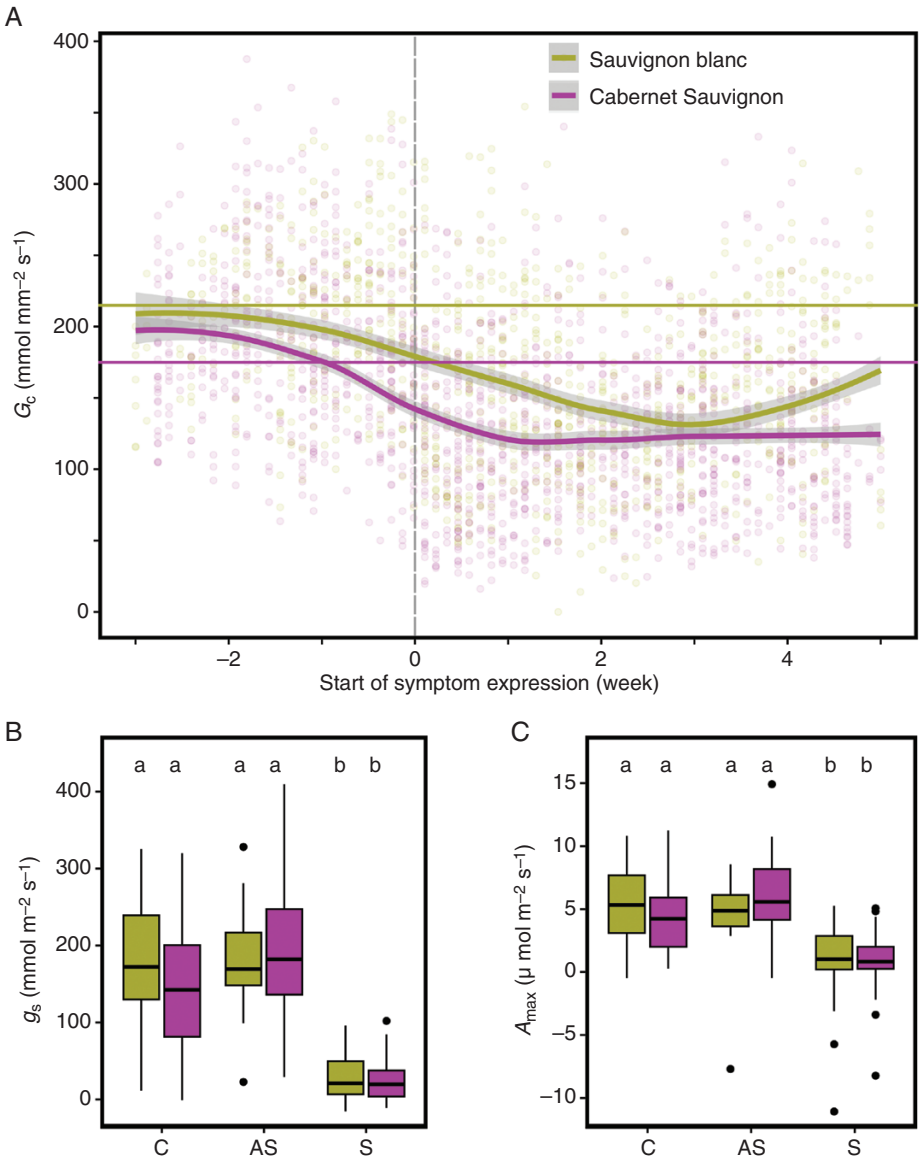

FIG. 8. Whole-plant and leaf physiology in control and esca-symptomatic *Vitis vinifera* cv. 'Sauvignon blanc' and 'Cabernet Sauvignon'. (A) Evolution of whole-plant (canopy) stomatal conductance (G_C, mmol m^{-2} s^{-1}) according to the beginning of esca symptom expression in weeks (0 corresponds to the first appearance of leaf symptoms). (B) Leaf stomatal conductance (g_s, mmol m^{-2} s^{-1}) measured with a porometer. (C) Net CO_2 leaf assimilation (A, µmol m^{-2} s^{-1}) measured with a gas analyser. Panels A and B present three types of leaves: 'C', leaves from control plants (asymptomatic between June and October 2021); 'AS', asymptomatic leaves from symptomatic plants (both before and after symptom appearance); and 'S', symptomatic leaves (presenting tiger-stripe symptoms). Sample sizes for stomatal conductance (B) were: 'Sauvignon blanc', $n = 37$ 'C', $n = 32$ 'S', $n = 12$ 'AS'; and 'Cabernet Sauvignon', $n = 32$ 'C', $n = 47$ 'S', $n = 24$ 'AS' leaves. Sample sizes for CO_2 assimilation were: 'Sauvignon blanc', $n = 36$ 'C', $n = 19$ 'S', $n = 25$ 'AS'; and 'Cabernet Sauvignon', $n = 26$ 'C', $n = 17$ 'S', $n = 38$ 'AS' leaves. Lower-case letters indicate statistical significance ($P < 0.05$); for more details see Supplementary Data Table S7.

of grape berries, as demonstrated by Van de Wal *et al*. (2018). Conversely, esca pathogenesis had a significant impact on stem growth patterns. Esca systematically perturbs growth dynamics when compared to the control pattern. Depending on the plant, the shrinkage phase can occur at the same time as or later than in control plants, can be absent, or can be observed multiple times over the season. The average growth rate during the shrinkage period ('SH', based on the control plants) was significantly higher in 'Sauvignon blanc' symptomatic plants (only one control stem was monitored in 'Cabernet Sauvignon'). One of the greatest difficulties in studying esca is that it is impossible to know at the beginning of the season which plants or stems will express symptoms and when. This explains, especially in the dendrometer analysis, the different sample sizes of control and symptomatic plants. Although we were able to use only a small number of trunk dendrometers, we observed similar trunk radial growth patterns as in stems (Supplementary Data Fig. S2).

The observed alteration in stem growth patterns were observed at a distance from the trunk where the esca-related pathogens are living (Bortolami *et al*., 2019). In other perennial species, a reduction in growth has been observed after inoculation with different pathogens (Cohen *et al*., 1997; Luque

et al., 1999), differing from our study by the proximity of the inoculation site to the position of the sensor used (placed 15 cm above). These authors also showed that the evolution of growth after inoculation was pathogen-dependent. The heterogeneous growth response we observed in symptomatic plants could be due to the fact that several esca-related pathogen species are associated with esca symptoms and/or to the heterogeneity of plant responses to their interactions with pathogens.

Xylem development adaptation during esca pathogenesis

The decrease in growth following pathogen inoculation (or, in our case, pathogen activity) could result from the occlusion of xylem vessels as suggested by Luque *et al*. (1999) and Cohen *et al*. (1997). The pathogenesis of plant diseases can be associated with anatomical changes in wood, especially in terms of vessel diameter, density and tylose production over years (Renzi *et al*., 2012; Sabella *et al*., 2020). To understand the alteration of the shrinkage period during esca pathogenesis, we explored the anatomical characteristics of stem xylem, specifically by categorizing the different types of vessels observed in xylem sectors from the pith to the outer part of the xylem.

Overall, symptomatic stems had a slightly higher percentage of tyloses (i.e. xylem occlusions) than control stems, and a significantly higher density of occluded vessels. This finding confirms previous results found in esca-symptomatic 'Sauvignon blanc' (Bortolami *et al*., 2021*a*) and in other vascular diseases, such as Pierce's disease caused by *Xylella fastidiosa* (Sun *et al*., 2013; Fanton *et al*., 2022). By dividing the dorso-ventral region of each stem into five intervals based on the distance from the pith, we conducted a more detailed spatial analysis of vessel density and diameter, as well as k_{ts} and PLC_{th}. We demonstrated that tylosis formation in control plants was low and restricted to the closest interval to the pith (i.e. protoxylem), where the vessels are predominantly small, <50 µm. By contrast, in esca-symptomatic stems, the density of occluded vessels was higher than in control stems in all intervals across the xylem area, suggesting a plant defence response.

Interestingly, symptomatic plants were able to produce non-occluded vessels late in the season (see examples in Supplementary Data Fig. S1), efficiently transporting sap as shown by dye infiltration [Fig. 4(i)]. Those vessels, observed above 60 % of the relative distance from the pith, were much smaller and at a higher density than vessels of control plants in the same xylem sector. The production of numerous small vessels in the xylem periphery has also been identified with flavescence dorée disease on the tolerant cultivar 'Merlot' but not on the susceptible cultivar 'Chardonnay' (Jelmini *et al*., 2021). In the context of abiotic stress (e.g. drought), the decrease in stem basal area during drought and then its increase following drought has already been associated with 'hydraulic repair' in response to embolism via the formation of new functional vessels in woody trees such as *Callitris* (Brodribb *et al*., 2010) and *Eucalyptus* (Gauthey *et al*., 2022). This suggests that after a drought, the cambium had the capacity to produce new vessels. In these two cases of biotic and abiotic stress, it appears that the ability to produce new vessels and thus new shoots helps to maintain productivity and enhance the likelihood of survival. This suggests that the alteration of the shrinkage phase during esca pathogenesis may be related to the preservation of cambial activity. Here, the formation of numerous small functional xylem vessels at the end of the season may have supported the formation of new healthy shoots, and compensated for the negative consequences of esca on plant growth dynamics, physiology, and xylem anatomy. The hypothesis of the positive influence of new green shoots on plant health is supported by previous research showing that esca did not negatively impact stem starch content in winter in untopped esca-symptomatic vines (Bortolami *et al*., 2021*b*). Vessel occlusion by tylosis is a phenomenon associated with ethylene production (Sun *et al*., 2007). This gaseous phytohormone, sometimes in association with other hormones such as auxin, stimulates cambial activity by acting through ethylene receptors (Sorce *et al*., 2013). Future research could study the importance of ethylene and the causal relationships between tylosis formation, growth alteration and the preservation of vessel formation.

Differential impact of esca on grapevine hydraulics among cultivars

Vessel size partly determines the plant water-carrying capacity by conditioning the hydraulic conductivity (Tyree and Zimmermann 2002). Hydraulic traits have been reported between cultivars (Villalobos-González *et al*., 2018; Dayer *et al*., 2020) and also during the development of vascular diseases (Sun *et al*., 2013; Bortolami *et al*., 2021*a*). Additionally, studies have demonstrated that cultivar variability can result in heterogeneous responses of hydraulic traits in the presence of a vascular pathogen (Deyett and Rolshausen, 2019; Fanton and Brodersen, 2021).

In our study, we showed that k_{ts} differed according to the grape cultivar, with a reduced k_{ts} ($k_{ts\ all\ vessels}$ and $k_{ts\ non\ occ.\ vessels}$) in 'Cabernet Sauvignon'. In addition, the development of esca led to a significantly higher theoretical percentage loss of conductivity (PLC_{th}) due to vessel occlusions in symptomatic stems than in control stems across intervals. The theoretical impact of vessel occlusions was also evidenced through a significantly higher $k_{ts\ occ.\ vessels}$ in symptomatic stems than in control stems. However, we did not identify any significant difference in k_{ts} ($k_{ts\ all\ vessels}$ and $k_{ts\ non\ occ.\ vessels}$) between symptomatic and control plants in either of the two grape cultivars. This can be explained by the variability in the percentage of occlusion in stem xylem vessels (Deyett and Rolshausen, 2019; Fanton and Brodersen, 2021). In addition, 50-µm cross-sections at a given vertical location in each section were analysed and we can assume that, in the case of symptomatic plants, some of the vessels defined as non-occluded may be actually occluded up- or downstream. Therefore, it is likely that we overestimated the contribution of non-occluded vessels to $k_{ts\ non\ occlu.\ vessels}$ and underestimated the compensatory effect of late functional vessel production. Tyloses occluding stem xylem vessels are responsible for hydraulic conductivity losses as shown, for example, in a root pathogen infecting pine trees (Mensah *et al*., 2020) and in esca disease (Bortolami *et al*., 2021*a*).

At the leaf level, we confirmed that esca symptoms are associated with significant levels of vessel occlusion in both cultivars (as also shown by Bortolami *et al*., 2023). However, the impact of these occlusions on gas exchange was still unclear. At the leaf level, we showed that leaf symptom onset was associated with a decrease in stomatal conductance and CO_2 assimilation in both cultivars. At the whole-plant level, we demonstrated that the onset of leaf symptoms was preceded by a decrease in canopy conductance (G_C) in both 'Sauvignon blanc' and 'Cabernet Sauvignon'. This pattern was previously shown in 'Sauvignon blanc' by Bortolami *et al*. (2021*b*), confirming the negative impact of esca on whole-plant gas exchange. We also confirmed that esca did not affect midday water potential and gas exchanges in asymptomatic leaves in either of the two cultivars, despite significant losses of conductivity in stems. The damage responsible for causing reductions in *Gc* is thus primarily localized within the symptomatic leaves. Both cultivars were able to produce new green leaves after pathogenesis, and we can link this capacity with the observed recovery of G_C in 'Sauvignon blanc' and the G_C stabilization in 'Cabernet Sauvignon'. This formation of new healthy shoots and G_C recovery may have been supported by the maintenance of cambial activity through the formation of numerous small functional xylem vessels at the end of the season. Symptomatic stems exhibit a certain degree of resilience to the disease, whereas leaves, crucial for growth, cannot recover and eventually die.

To conclude, we have shown that esca pathogenesis altered the shrinkage phase during stem growth, probably through modified vascular cambial activity. Symptomatic plants were able to compensate for the negative impacts of esca on leaves, especially on stomatal and canopy conductance. We hypothesize that stem xylem occlusions and the subsequent localized loss of conductivity in symptomatic stems could trigger the production of new numerous small xylem vessels associated with new healthy shoots at the end of the season. These results suggest that grapevine has resilience mechanisms that could play a crucial role in its defence against esca. The mechanisms underlying the modification of cambial activity during esca pathogenesis remain unknown and are a promising area for further research. It will be essential to study these responses on a wider range of grape cultivars more or less sensitive to this disease in similar contexts. Comparing different levels of plant vigour, either in the field or in potted plants, could also be an important field of research to investigate the impact of vigour on resilience capacity. In cultivated vineyards, topping is a common procedure used several times during the year to maintain a constant vegetative surface and to allow the passage of vineyard machinery. However, in a vineyard highly infected by esca, this practice could play a negative role by removing new photosynthetically active 'organs' produced by the symptomatic plants in the weeks following symptom development, thus preventing a recovery of gas exchange and photosynthetic activity that contribute to the maintenance of carbohydrate reserves.

SUPPORTING INFORMATION

Supplementary data are available online at https://academic.oup.com/aob and consist of the following.

Fig. S1. Photographs of whole plants, leaves and cross-sections of esca-symptomatic or control plants of *Vitis vinifera* cv. 'Sauvignon blanc' and 'Cabernet Sauvignon'. Fig. S2. Evolution of the standardized maximum daily diameter (*MXD* in μm) of different trunks, during one vegetative season, in *Vitis vinifera* cv. 'Sauvignon blanc' and 'Cabernet Sauvignon'. Fig. S3. Stem xylem anatomy in *Vitis vinifera* cv. 'Sauvignon blanc' and 'Cabernet Sauvignon' control plants. Fig. S4. Relationships between theoretical specific hydraulic conductivity and normalized distance to the pith (%) in symptomatic and control stems of 'Sauvignon blanc' and 'Cabernet Sauvignon', when considering either non-occluded vessels (A) or occluded vessels (B). Fig. S5. Evolution of whole-plant (canopy) stomatal conductance (G_C, mmol m^{-2} s^{-1}) of control plants during the season in *Vitis vinifera* cv. 'Sauvignon blanc' and 'Cabernet Sauvignon'. Fig. S6. Midday water potentials measured on different types of 'Sauvignon blanc' and 'Cabernet Sauvignon' leaves. Table S1. Effect of esca leaf symptoms and growth period (GR, SH, ST) on the average weekly daily growth rate (DGR_W) in 'Sauvignon blanc'. Table S2. Comparative analysis of xylem anatomical characteristics in 'Sauvignon blanc' and 'Cabernet Sauvignon' control stems, and in control and esca-symptomatic stems within each cultivar using ANOVAs. Table S3. Effect of normalized distance from the pith, cultivar and esca leaf symptoms on vessel density (V_D, estimated from non-occluded vessels and occluded vessels). Table S4. Effect of normalized distance from the pith, cultivar and esca leaf symptoms on vessel size. Table S5. Effect of normalized distance from the pith, cultivar and esca leaf symptoms on k_{ts} (estimated for all vessels, non-occluded vessels and occluded vessels only). Table S6. Effect of normalized distance from the pith, cultivar and esca leaf symptoms on the theoretical percentage loss of conductivity (PLC_{th}). Table S7. Effect of cultivar and esca leaf symptoms on g_s and A. Table S8. Effect of cultivar and esca leaf symptoms on midday water potentials.

FUNDING

This work was supported by the projects PHYSIOPATH (22001150) and ESCAPADE (22001436) (programme 'Plan National Dépérissement du Vignoble', FranceAgriMer/CNIV) and the Nouvelle-Aquitaine region (project VITIPIN, 22001439).

ACKNOWLEDGMENTS

We thank the experimental teams of UMR SAVE and UMR EGFV (INRAE, Bordeaux, France) for providing materials, logistics and assistance during the experimentation. We thank Jérôme Jolivet and Sebastien Gambier (UMR SAVE) for providing technical knowledge and support for plant transplantation and maintenance. We thank Nabil Girollet, Guillaume Pacreau and Nabil Zirari for maintenance of the mini-lysimeter glasshouse phenotyping platform (Bord'O platform, INRAE Bordeaux). We thank Régis Burlett and Patrick Leger for expertise, support and materials with the dendrometer.

CONFLICT OF INTEREST

The authors declare that they have no competing interests in relation to this study.

AUTHOR CONTRIBUTIONS

C.E.L.D., G.A.G., N.D.A., S.D., L.L. and N.S. designed the experiments; N.D.A., C.E.L.D. and N.F. conducted the esca symptom notations; N.D.A. and N.F. carried out the samplings, managed the dendrometers over the season, and measured leaf gas exchange and leaf area; N.D.A., N.F. and C.E.L.D measured midday water potentials; P.T. and N.F. conducted the histological preparation; N.D.A. and P.T. processed the optical images in ImageJ; N.D.A. analysed optical images and data sets from balances, leaf areas, dendrometers, weather stations, leaf gas exchange and water potentials; N.D.A., C.E.L.D., and G.A.G. wrote the article; all authors edited and agreed on the final version of the article.

DATA AVAILABILITY

Raw datasets are available in the INRAE dataverse: https://doi.org/10.57745/V1C8MJ, Recherche Data Gouv, V1.

REFERENCES

Bortolami G, **Gambetta GA**, **Delzon S**, ***et al***. **2019**. Exploring the hydraulic failure hypothesis of esca leaf symptom formation. *Plant Physiology* **181**: 1163–1174.

Bortolami G, **Farolfi E**, **Badel E**, ***et al***. **2021***a*. Seasonal and long-term consequences of esca grapevine disease on stem xylem integrity. *Journal of Experimental Botany* **72**: 3914–3928.

Bortolami G, **Gambetta GA**, **Cassan C**, ***et al***. **2021***b*. Grapevines under drought do not express esca leaf symptoms. *Proceedings of the National Academy of Sciences of the United States of America* **118**: e2112825118.

Bortolami G, **Ferrer N**, **Baumgartner K**, ***et al***. **2023**. Esca grapevine disease involves leaf hydraulic failure and represents a unique premature senescence process. *Tree Physiology* **43**: 441–451.

Brodribb TJ, **Bowman DJMS**, **Nichols S**, **Delzon S**, **Burlett R. 2010**. Xylem function and growth rate interact to determine recovery rates after exposure to extreme water deficit. *The New Phytologist* **188**: 533–542.

Bruez E, **Lecomte P**, **Grosman J**, ***et al***. **2013**. Overview of grapevine trunk diseases in France in the 2000s. *Phytopathologia Mediterranea* **52**: 262–275.

Cailleret M, **Jansen S**, **Robert EMR**, ***et al***. **2017**. A synthesis of radial growth patterns preceding tree mortality. *Global Change Biology* **23**: 1675–1690.

Cohen M, **Luque J**, **Alvarez IF. 1997**. Use of stem diameter variations for detecting the effects of pathogens on plant water status. *Annales des Sciences Forestières* **54**: 463–472.

Collins BR, **Parke JL**, **Lachenbruch B**, **Hansen EM. 2009**. The effects of *Phytophthora ramorum* infection on hydraulic conductivity and tylosis formation in tanoak sapwood. *Canadian Journal of Forest Research* **39**: 1766–1776.

Conesa MR, **Dodd IC**, **Temnani A**, **De la Rosa JM**, **Pérez-Pastor A. 2018**. Physiological response of post-veraison deficit irrigation strategies and growth patterns of table grapes (cv Crimson Seedless). *Agricultural Water Management* **208**: 363–372.

Daudet F-A, **Améglio T**, **Cochard H**, **Archilla O**, **Lacointe A. 2005**. Experimental analysis of the role of water and carbon in tree stem diameter variations. *Journal of Experimental Botany* **56**: 135–144.

Dayer S, **Herrera JC**, **Dai Z**, ***et al***. **2020**. The sequence and thresholds of leaf hydraulic traits underlying grapevine varietal differences in drought tolerance. *Journal of Experimental Botany* **71**: 4333–4344.

De Micco V, **Balzano A**, **Wheeler EA**, **Baas P. 2016**. Tyloses and gums: a review of structure, function and occurrence of vessel occlusions. *IAWA Journal/International Association of Wood Anatomist* **37**: 186–205.

Deslauriers A, **Rossi S**, **Anfodillo T. 2007**. Dendrometer and intra-annual tree growth: what kind of information can be inferred? *Dendrochronologia* **25**: 113–124.

Deyett E, **Rolshausen PE. 2019**. Temporal dynamics of the sap microbiome of grapevine under high Pierce's disease pressure. *Frontiers in Plant Science* **10**: 1246.

Dixon HH, **Joly J. 1894**. On the ascent of sap. *Proceedings of the Royal Society of London* **57**: 3–5.

Ewers B, **Oren R. 2000**. Analyses of assumptions and errors in the calculation of stomatal conductance from sap flux measurements. *Tree Physiology* **20**: 579–589.

Fanton AC, **Brodersen C. 2021**. Hydraulic consequences of enzymatic breakdown of grapevine pit membranes. *Plant Physiology* **186**: 1919–1931.

Fanton AC, **Furze ME**, **Brodersen CR. 2022**. Pathogen-induced hydraulic decline limits photosynthesis and starch storage in grapevines (*Vitis sp*). *Plant, Cell & Environment* **45**: 1829–1842.

Fernández JE, **Cuevas MV. 2010**. Irrigation scheduling from stem diameter variations: A review. *Agricultural and Forest Meteorology* **150**: 135–151.

Gärtner H, **Lucchinetti S**, **Schweingruber F. 2014**. New perspectives for wood anatomical analysis in dendrosciences: the GSL1-microtome. *Dendrochronologia* **32**: 47–51.

Gauthey A, **Peters JMR**, **Lòpez R**, ***et al***. **2022**. Mechanisms of xylem hydraulic recovery after drought in *Eucalyptus saligna*. *Plant, Cell & Environment* **45**: 1216–1228.

Gruber A, **Oberhuber W**, **Wieser G. 2018**. Nitrogen addition and understory removal but not soil warming increased radial growth of *Pinus cembra* at treeline in the Central Austrian Alps. *Frontiers in Plant Science* **9**: 711.

Hartmann H, **Messier C. 2008**. The role of forest tent caterpillar defoliations and partial harvest in the decline and death of sugar maple. *Annals of Botany* **102**: 377–387.

Hofstetter V, **Buyck B**, **Croll D**, **Viret O**, **Couloux A**, **Gindro K. 2012**. What if esca disease of grapevine were not a fungal disease? *Fungal Diversity* **54**: 51–67.

Intrigliolo D, **Castel J. 2007**. Evaluation of grapevine water status from trunk diameter variations. *Irrigation Science* **26**: 49–59.

Jelmini L, **Rizzoli A**, **Jermini M**, **Schumpp O**, **Conedera M. 2021**. Phloem and xylem modifications of *Vitis vinifera* stems in response to flavescence dorée phytoplasma infection. *Plant Pathology* **70**: 970–979.

Luque J, **Cohen M**, **Savé R**, **Biel C**, **Álvarez IF. 1999**. Effects of three fungal pathogens on water relations, chlorophyll fluorescence and growth of *Quercus suber* L. *Annals of Forest Science* **56**: 19–26.

McDowell NG, **Sapes G**, **Pivovaroff A**, ***et al***. **2022**. Mechanisms of woody-plant mortality under rising drought, CO_2 and vapour pressure deficit. *Nature Reviews Earth & Environment* **3**: 294–308.

Mensah JK, **Sayer MAS**, **Nadel RL**, **Matusick G**, **Eckhardt LG. 2020**. Physiological response of *Pinus taeda* L. trees to stem inoculation with *Leptographium terebrantis*. *Trees* **34**: 869–880.

Mugnai L, **Graniti A**, **Surico G. 1999**. Esca (black measles) and brown wood-streaking: two old and elusive diseases of grapevines. *Plant Disease* **83**: 404–418.

Oliva J, **Stenlid J**, **Grönkvist-Wichmann L**, ***et al***. **2016**. Pathogen-induced defoliation of *Pinus sylvestris* leads to tree decline and death from secondary biotic factors. *Forest Ecology and Management* **379**: 273–280.

Pearce RB. 1996. Antimicrobial defences in the wood of living trees. *The New Phytologist* **132**: 203–233.

Renzi M, **Copini P**, **Taddei AR**, ***et al***. **2012**. Bacterial canker on kiwifruit in Italy: anatomical changes in the wood and in the primary infection sites. *Phytopathology* **102**: 827–840.

Rioux D, **Nicole M**, **Simard M**, **Ouellette GB. 1998**. Immunocytochemical evidence that secretion of pectin occurs during gel (gum) and tylosis formation in trees. *Phytopathology* **88**: 494–505.

Rizzoli A, **Jelmini L**, **Pezzatti G**, ***et al***. **2022**. Impact of the 'Flavescence Dorée' phytoplasma on xylem growth and anatomical characteristics in trunks of 'Chardonnay' Grapevines (*Vitis vinifera*). *Biology* **11**: 978.

Rudelle J, **Octave S**, **Kaid-Harche M**, **Roblin G**, **Fleurat-Lessard P. 2005**. Structural modifications induced by *Eutypa lata* in the xylem of trunk and canes of *Vitis vinifera*. *Functional Plant Biology* **32**: 537–547.

Sabella E, **Moretti S**, **Gärtner H**, ***et al***. **2020**. Increase in ring width, vessel number and δ18O in olive trees infected with *Xylella fastidiosa*. *Tree Physiology* **40**: 1583–1594.

Scholz F, **Bucci S**, **Goldstein G**, **Meinzer F**, **Franco A**, **Miralles-Wilhelm F. 2008**. Temporal dynamics of stem expansion and contraction in savanna trees: withdrawal and recharge of stored water. *Tree Physiology* **28**: 469–480.

Scholz A, **Klepsch M**, **Karimi Z**, **Jansen S. 2013**. How to quantify conduits in wood? *Frontiers in Plant Science* **4**: 56.

Sorce C, **Giovannelli A**, **Sebastiani L**, **Anfodillo T. 2013**. Hormonal signals involved in the regulation of cambial activity, xylogenesis and vessel patterning in trees. *Plant Cell Reports* **32**: 885–898.

Sun Q, **Rost TL**, **Reid MS**, **Matthews MA. 2007**. Ethylene and not embolism is required for wound-induced tylose development in stems of grapevines. *Plant Physiology* **145**: 1629–1636.

Sun Q, **Sun Y**, **Walker MA**, **Labavitch JM. 2013**. Vascular occlusions in grapevines with Pierce's disease make disease symptom development worse. *Plant Physiology* **161**: 1529–1541.

Tyree MT, **Zimmermann MH. 2002**. Conducting units: Tracheids and vessels. In: **Tyree MT**, **Zimmermann MH**, eds. *Xylem structure and the ascent of sap*. Berlin: Springer, 1–25.

Urban J, **Dvořák M. 2014**. Sap flow-based quantitative indication of progression of Dutch elm disease after inoculation with *Ophiostoma novo-ulmi*. *Trees* **28**: 1599–1605.

Van de Wal BAE, **Leroux O**, **Steppe K. 2018**. Post-veraison irreversible stem shrinkage in grapevine (*Vitis vinifera*) is caused by periderm formation. *Tree Physiology* **38**: 745–754.

Villalobos-González L, **Quintana-Pulido C**, **Muñoz M**, **Franck N**, **Pastenes C. 2018**. Xylem structure and function in three grapevine varieties. *Chilean Journal of Agricultural Research* **78**: 419–428.

Yadeta KA, **Thomma BPHL. 2013**. The xylem as battleground for plant hosts and vascular wilt pathogens. *Frontiers in Plant Science* **4**: 97.